Photoemission Spectroscopy of Tethered CdSe Nanocrystals: Shifts in Ionization Potential and Local Vacuum Level As a Function of Nanocrystal Capping Ligand

Andrea M. Munro,* Brian Zacher, Amy Graham, and Neal R. Armstrong*

Department of Chemistry, University of Arizona, Tucson, Arizona 85721

ABSTRACT We report the characterization of the frontier orbital energies and interface dipole effects for bare and ligand-capped 3.6 and 6.0 nm diameter CdSe nanocrystals (NC) tethered to smooth gold substrates, using He(I) and He(II) UV photoemission spectroscopy. Changes in the ionization potential (IP) of the NCs and local effective work function of the films were explored as a function of the dipolar nature of the NC capping ligands. The addition of thiol-capping ligands 1-hexanethiol, 1-benzenethiol, and 4-fluorothiophenol to both sizes of NCs produces negligible shifts in energy offset between the high kinetic energy edge of the CdSe NCs and the gold substrate Fermi energy. However, the local vacuum level and IP of the nanocrystal layer are altered by as much as 0.3 eV. We demonstrate the importance of determining both the local vacuum level and the high kinetic energy edge of a tethered NC sample. These studies demonstrate a method that can be used in the future to characterize the frontier orbital energy offsets for modified or unmodified nanocrystalline films, in which the NCs are incorporated into host materials, for applications ranging from photovoltaics to light-emitting diodes.

KEYWORDS: semiconductor nanocrystal • self-assembled monolayer • UV-photoelectron spectroscopy ionization potential • dipole moment • vacuum level shift

INTRODUCTION

Semiconductor nanocrystals (NCs) are increasingly used as emissive dopants in light-emitting diodes (1−4), as light absorbing, electron transporting materials in polymer/NC hybrid photovoltaics (PVs) (5, 6), and as both donor and acceptor materials in all-inorganic NC photovoltaics (7, 8). Further optimization of these technologies requires a better understanding of changes in NC ionization potential (IP or valence band energy) and electron affinity (EA or conduction band energy) as a function of NC diameter and shape. It is also important to understand changes in IP and EA due to NC−NC interactions in closely packed NC assemblies, and the interaction between NCs and their local environment, especially the nature of capping ligands or host polymers or small molecules (9−13).

The organic capping ligands that surround a NC form a dielectric layer that may electronically and energetically isolate a NC from the local environment, if a truly close-packed array of ligands is formed on the NC surface (14−20). Changing the organic capping ligands affects NC solubility (21, 22), photoluminescence efficiency and excited state lifetimes (17, 23−25), and charge transport between NCs (26−28). It has been hypothesized that certain ligands may also alter the valence and conduction band energies of colloidal NCs (11, 12). Attempts to quantitatively characterize these effects have recently been carried out using electrochemical and spectroscopic measurements in combination with scanning tunneling spectroscopy of single NCs by Soreni-Harari et al. (12). In this paper, we will discuss how the IP and effective work function of single monolayers of CdSe NCs are affected by the NC capping ligands, as revealed by He(I) and He(II) UV photoemission spectroscopy (UPS).

Colvin, Alivisatos, and Tobin initially showed that CdS NCs could be tethered to gold surfaces as compact monolayers, using 1,6-hexanedithiol (HDT) as the tether (29). Using a synchrotron excitation source (20−70 eV excitation energies), they measured shifts in the high kinetic energy edge of the surface (without considering local vacuum level shifts) as a function of NC diameter. The authors reported a shift of 0.7 eV for 2.5 nm NCs relative to 7.0 nm NCs. Subsequent photoemission studies by Wu et al. (30, 31) have focused on multilayer assemblies, using CdSe NCs capped with pyridine or a mixture of hexadecylamine and tri-*n*-octylphosphine oxide (TOPO), and have attributed some of the shifts in the frontier orbital energies to final-state effects. Meulenberg et al. (32) reported that they did not observe final-state effects for CdSe NCs films when they performed photoemission spectroscopy to measure the exciton binding energy of CdSe NCs with varying diameter. They attributed these differences in data interpretation to the fact that each group referenced their photoemission data to different "bulk" CdSe standards.

Guyot-Sionnest and co-workers (33, 34) performed spectroelectrochemistry of CdSe multilayers on platinum electrodes for 3.0, 5.4, and 7.0 nm diameter TOPO-capped CdSe

* To whom correspondence should be addressed. E-mail: nra@email.arizona.edu (N.R.A); ammunro@email.arizona.edu (A.M.M.).
Received for review November 27, 2009 and accepted February 1, 2010

DOI: 10.1021/am900834y

NCs, and found the first reduction potential to be −0.80 V vs SHE for the 7.0 nm NCs (implying an EA of 3.70 eV for films created from the largest diameter NCs in contact with electrolyte solutions, assuming that the SHE potential versus vacuum ≈ −4.5 eV) (35). The first reduction potential of the 7.0 nm NC multilayer film changed from −0.8 to −1.07 V vs SHE (i.e., EA ≈ 3.70 to 3.43 eV) after exchanging the TOPO capping ligands with 1-octanethiol, implying that the capping ligand may add or subtract from the effective band edge energies of the NC, or that they raise or lower additional energy barriers to charge injection to and from the NC.

Soreni-Harari et al. have recently proposed that the conduction and valence band energies of InAs NCs appear to be shifted by exchanging the capping ligand (12). They used electrochemical methods and scanning tunneling spectroscopies of single NCs to characterize these shifts. Although the absorbance spectrum of the NCs (and thus the optical band gap) was constant as the surface ligands were exchanged, the first reduction potential of a NC film was altered. Thus the authors proposed that exchanging the NC surface ligands shifted both the IP and EA energies of the NCs by an equal amount. They did not observe a correlation between the shift in reduction potential and the dipolar nature of each ligand.

Similarly, Campbell et al. (36), using electroabsorption spectroscopy of blends of NCs and poly(9,9-dioctylfluorene), reported that the EA and IP of CdSe/ZnS NCs were 3.9 and 5.9 eV, respectively. From these studies it is apparent that a dipole layer was formed at the NC-polymer interface. Shalom et al. (11) also showed that changing the surface ligands on CdS NCs grown directly onto TiO_2 (in CdS sensitized TiO_2 photoelectrochemical cells) altered the onset of the photovoltage spectrum for the device by up to 0.2 eV. The shift in the photovoltage spectrum was shown to correlate with the dipole moment of the various ligands used in the study. Zhu and co-workers recently extended the study of NCs tethered to metal oxide surfaces to include the characterization of CdSe NC monolayers on single-crystal ZnO, where an argument was made for pinning of valence band energy on the oxide surface (37).

In this paper, we return to the initial approach of Colvin et al. (29), tethering CdSe NCs to template-stripped ultrasmooth gold surfaces, and probing their frontier orbital energies with He(I) and He(II) UPS, for NCs with different capping ligands (Figure 1). We use protocols developed to examine interface dipole effects induced by self-assembled dipolar monolayers on gold, silver, and indium−tin oxide (ITO) surfaces (38−42). The sampling depth afforded by He(I) and He(II) photoemission is on the order of 3−5 nm (3−5 times the inelastic mean free path of the photoelectrons), but traces of Fermi edge photoemission from the underlying gold substrate and dithiol tether remain observable, allowing us to confirm that charging of the NC film does not occur (i.e., that electronic equilibrium between the spectrometer and the sample is maintained). We can resolve the high kinetic energy edge for the NCs separate from the underlying substrate and modifier and account for changes

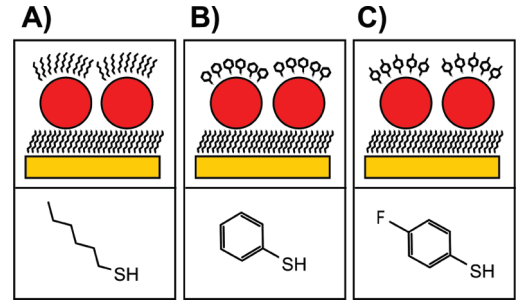

FIGURE 1. Schematic of samples with CdSe NCs tethered to gold with a 1,6-hexanedithiol (HDT) self-assembled monolayer (SAM). The capping ligands varied for each sample: (A) 1-hexanethiol (HT), (B) 1-benzenethiol (BT), and (C) 4-fluorthiophenol (FTP).

in the local vacuum level, to provide a corrected IP for the bound NCs. Subsequent additions of various thiol capping ligands produce only small changes in the high kinetic energy edge of the NC photoemission spectrum, but sizable changes in the local vacuum level are observed, as shown by shifts in the low kinetic energy edge of the photoemission spectrum. Varying the capping ligands (Figure 1), provides reasonable differences in molecular dipole moment, and can shift the IP of the CdSe NC, corrected for changes in local vacuum level, by up to 0.3 eV. The shift in vacuum level of the surface as a function of the dipolar nature of the ligand is analogous to the vacuum level shifts previously observed when small molecule modifiers are bound to metallic and semiconductor surfaces (38−42).

EXPERIMENTAL SECTION

All chemicals were purchased from Sigma-Aldrich and used as received. For the studies of ligand capping effects, two batches of ligand-capped CdSe NCs with diameters of 3.6 and 6.0 nm were synthesized by previously reported methods, with sizes confirmed spectroscopically (24, 43). After synthesis the NCs were extracted 2 times using hexanes and methanol, then washed 3 times by suspending the NCs in toluene and precipitating them with acetone and centrifugation. After washing, the NCs were pyridine exchanged by suspending the NCs in neat pyridine and precitating with hexanes and centrifugation as previously reported (5, 44). This exchange procedure was performed 3 times on each batch of NCs to ensure complete removal of TOPO, oleic acid, and octadecylamine ligands, leaving pyridine-capped NCs (pyr-CdSe).

On the day of the experiment, template-stripped gold (rms roughness 0.5 nm, determined by AFM) was removed from a silicon substrate by cutting along the edges with a razor blade and peeling the substrate up (45). Template-stripped gold was fabricated by thermal evaporation of 200 nm of gold (Kurt J. Lesker) onto silicon substrates (Silicon Quest International, item #707−005). After the substrates were allowed to cool and were brought back to atmosphere, glass substrates were attached to the gold with epoxy (Epoxy Technology (EPO-TEK) 353ND4). The epoxy was cured by heating at 150 °C for at least 15 min. Substrates were stored until needed. After the gold substrate was removed from silicon on the day of the experiment, it was rinsed with ethanol and blown dry. Next, the substrate was oxygen plasma cleaned for 2 min (Harrick PDC-32G at 18W) and immediately immersed in a 1 mM HDT ethanoic solution for 30 min to 4 h to allow a self-assembled monolayer to form. After being soaked, the substrate was rinsed well with ethanol and blown dry. It was then soaked in a solution of pyr-CdSe NCs ([NC] > 1×10^{-6} M calculated as reported by Yu et al. (43)) in

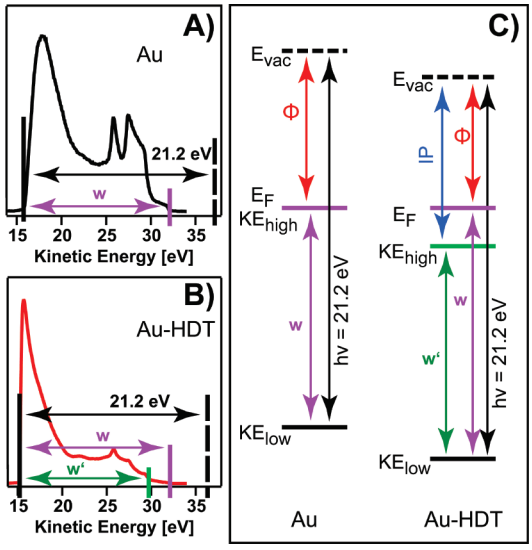

FIGURE 2. UPS spectra of (A) template-stripped Au and (B) a 1,6-hexanedithiol SAM on template-stripped Au. The width between the low kinetic energy edge and the local vacuum energy (21.2 eV) is labeled in black. The width between the low kinetic energy edge and the Fermi energy is labeled in purple (*w*). The width between the low kinetic energy edge and the high kinetic energy edge for the Au-HDT surface is labeled in green (*w*′). (C) Band diagrams of the surfaces in A and B indicating *w*, *w*′, the surface work function (Φ), and the IP.

methanol for an additional 30 min. The sample was then rinsed well with ethanol and blown dry. Finally, for those studies requiring the additional capping ligand, the samples were soaked in a 1 mM solution of either, 1-benzenethiol, 1-hexanethiol, or 4-fluorothiophenol for 1 h, rinsed well with ethanol, blown dry, and loaded into ultrahigh vacuum for photoemission spectroscopy measurements.

UPS was performed using a Kratos Axis-Ultra spectrometer. For the UPS experiments, both He(I) (21.2 eV) and He(II) (40.8 eV) were used as the excitation source with a pass energy of 5 eV. A 9 V bias was applied between the sample and the detector to increase the kinetic energy of the lowest kinetic energy photoelectrons into an energy region favoring their analysis and detection. The chamber pressure was 3×10^{-8} Torr. The Fermi energy for the spectrometer was determined using an argon sputtered, template-stripped gold sample with a work function of 5.1 eV, and in all subsequent experiments we observed the residual photoemission from the underlying gold substrate to confirm that electronic equilibrium between the sample and the spectrometer was maintained. All photoemission spectra were acquired at a normal takeoff angle.

Dipole moments for each modifier were calculated using the Spartan package using the 6-31G* basis set. Each molecule was geometry optimized in the gas phase at 298K keeping the thiol (H−S) intact, but with the bond angle = 0° (see the Supporting Information).

RESULTS AND DISCUSSION

UPS of Thiol Self-Assembled Monolayers. Panels A and B in Figure 2 show the He(I) photoemission spectra of a template-stripped gold surface and of a template-stripped gold surface with an HDT self-assembled monolayer, respectively. The local work function and IP were determined by methods reviewed by Cahen and Kahn (46) and Seki and co-workers (47). We assume that electronic equilibrium is maintained between the substrate and the spectrometer, thus the Fermi energy is constant. In UPS experiments, the local work function is defined as the difference between the local vacuum energy and the Fermi energy of the surface, while the IP is the difference in the local vacuum energy and the high kinetic energy edge for photoemission, as shown in Figure 2C. In the case of metal surfaces like gold, the local work function and the IP are equivalent, but for semiconductor and insulating samples, the IP is larger than the local work function of a given sample. The local vacuum energy is determined by the low kinetic energy (or the secondary electron edge), so that

$$\phi = h\nu - (E_{\text{Fermi}} - KE_{\text{low}}) \quad (1)$$

$$\text{IP} = h\nu - (KE_{\text{high}} - KE_{\text{low}}) \quad (2)$$

where ϕ is the local work function, E_{Fermi} is the Fermi energy, KE_{high} and KE_{low} are the high and low kinetic energy edges, respectively, and $h\nu$ is 21.2 and 40.8 eV for He(I) and He(II) photoemission experiments, respectively. The low kinetic energy edge contains the information about electrons that have either been scattered or that have a binding energy equal to the photon energy of the excitation source. So shifts in the low kinetic energy edge to lower values indicate downward shifting in the local vacuum level, and thus the local work function of a surface decreases.

It has been shown previously that the adsorption of self-assembled monolayers on metal and semiconductor surfaces can change the work function of the surface and that the shift in work function correlates with the dipole moments of the molecules that comprise the self-assembled monolayer (38−42, 48). Brédas and co-workers have hypothesized that the total dipole of a self-assembled monolayer on a metal surface can be considered as the sum of the molecular dipole, the dipole created by physisorption of material onto the metal surface, and the dipole created by the metal−thiol bond (48). In Figure 3, we plot the UPS data for each of the thiol-capping ligands tethered to template-stripped gold along with energy band diagrams of each surface. The local work function of gold with each adsorbed ligand are summarized in Table 1, along with the calculated dipole moment of each ligand in the unbound state determined by Spartan (see the Supporting Information). The change in the dipole moment of each ligand correlates with the local work function of gold after adsorption of each ligand. The exact magnitude of the shift in the work function depends on the packing density of the ligands on the surface and the orientation of the dipole moment of the ligands.

UPS Studies of CdSe NC Monolayers. Determination of the IP of CdSe NCs tethered to template-stripped gold is challenging because of the photoemission features associated with the underlying thiol tether (38, 39). We first analyze the surface work function, IP, and high kinetic energy edge for photoemission from bare, 6.0 nm diameter CdSe NCs tethered to template-stripped gold with HDT (Figure 4). We note that the pyridine-capping ligands are removed in ultrahigh vacuum (because of the lack of observ-

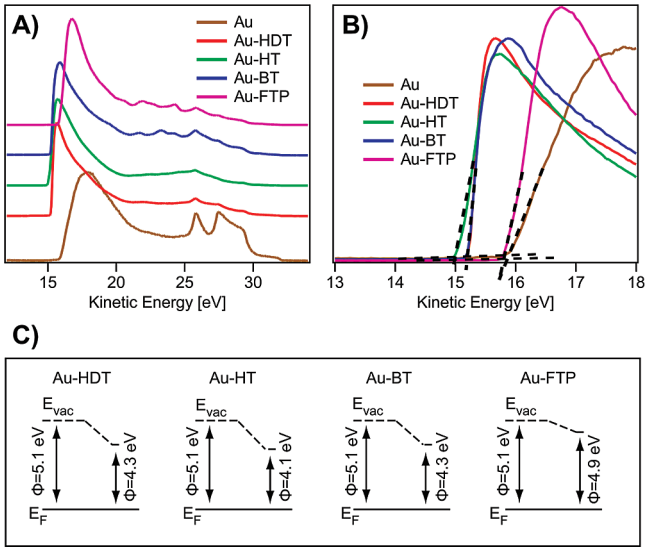

FIGURE 3. (A) He(I) UPS spectra of template-stripped gold (dark yellow) and template-stripped gold with different SAM layers; 1,6-hexanedithiol (red), 1-hexanethiol (green), 1-benzenethiol (blue), and 4-fluorothiophenol (purple). (B) Low kinetic energy edge of the spectra in A. (C) Band diagrams showing how the adsorption of each ligand shifts the local vacuum energy of the gold surface.

able nitrogen by X-ray photoelectron spectroscopy from these NC monolayers) confirming the observations of Katari et al. (49). We conclude that by tethering pyridine-capped NCs, we can collect spectra of bare NCs with no noticeable oxidation of the cadmium surface atoms on the NCs in ultrahigh vacuum (see XPS spectra in the Supporting Information). From analysis of the AFM data for these NC film on HDT/Au surfaces (see section S6 in Supporting Information) we estimate the surface coverage of NCs to be ca. 13−26% of a close-packed monolayer, with an average spacing between NCs of ca. 6−9 nm. We performed background subtraction of the UPS spectra in order to determine the high kinetic energy edge and IP of the tethered NCs. A weighted version of the UPS spectrum of a template-stripped gold substrate modified with a self-assembled monolayer of HDT was removed from the UPS spectrum of the CdSe NCs tethered to gold. The weighting factor takes into account the differences in signal intensity expected from HDT features alone, versus their intensity from below the CdSe NC layer (see the Supporting Information).

The low kinetic energy and high kinetic energy regions of the He(I) (21.2 eV) and He(II) (40.8 eV) UPS spectra for 6.0 nm CdSe NCs tethered to template-stripped gold capped with no ligand, 1-hexanethiol, 1-benzenethiol, or 4-fluorothiophenol are plotted in Figure 4, along with proposed band diagrams of each surface (full UPS spectra can be found in the Supporting Information). Both He(I) and He(II) photoemission spectra were used to characterize the surface since the resultant photoemission spectra probe different depths into the NC monolayer, and certain photoemission peaks have higher photoionization cross sections with the higher energy excitation source. For example, the Cd 3d peak can be observed with He(II), but not He(I) excitation. By performing the experiment with both excitation energies and using weighted background subtraction (see the Supporting Information), we determine a consistent high kinetic energy edge and IP for the NCs in each sample. We find that the IP of 6.0 nm diameter CdSe NCs tethered to a gold substrate with HDT is 6.2 ± 0.1 eV with an effective surface work function of the NC assembly of 4.2 ± 0.1 eV. Binding 1-hexanethiol to the surface of the NCs shifts the IP from 6.2 eV to 6.1 ± 0.1 eV. Similarly, the IP of tethered CdSe with 1-benzenethiol as the capping ligand is 6.2 ± 0.1 eV. Although the NC IP does not shift when either 1-hexanethiol or 1-benzenethiol is bound to the NC surface, the energy offset between the Fermi energy of clean gold and the IP of the NCs increases by 0.2 eV and the surface work function decreases (Figure 4D). In contrast, the IP of 6.0 nm diameter CdSe NCs capped with 1,4-fluorothiophenol is 6.5 ± 0.1 eV. This shift of 0.3 eV, occurs due to a shift in the local vacuum level and there is no change in the energy level offset between the NC high kinetic energy edge and the Fermi energy of gold (Figure 4B). We observe the same changes for both He(I) and He(II) excitation. The work function of each surface is summarized in Table 1 and the IP of the NCs is summarized in Table 2.

In Figure 5, the low kinetic energy and high kinetic energy regions of the He(I) and He(II) UPS spectra and band diagrams of tethered 3.6 nm diameter CdSe NCs capped with 1-hexanethiol, 1-benzenethiol, and 1,4-fluorothiophenol are shown (full UPS spectra can be found in the Supporting Information). The IPs of the CdSe NCs with each capping ligand are 6.2 ± 0.1 eV, 6.3 ± 0.1 eV, and 6.3 ± 0.1 eV (Table 2), whereas the surface work function for each sample is 4.1 ± 0.1 eV, 4.1 ± 0.1 eV, and 4.3 ± 0.1 eV (Table 1) for 1-hexanethiol, 1-benzenethiol, and 4-fluorthiophenol capping ligands, respectively. Although there is no significant change in the ionization potential of the CdSe NCs, we still observe a small shift in the local vacuum energy after ligand adsorption that is consistent with the shift observed for the ligands on 6.0 nm diameter NCs and for the ligands on gold although smaller in magnitude.

As mentioned above, the shifts in the local vacuum energy after ligand adsorption are smaller when the ligands are bound to tethered CdSe nanocrystals compared to gold. The shifts are also noticeably smaller for samples with 3.6 nm diameter NCs compared to samples with 6.0 nm diameter NCs. We attribute this to differences in surface roughness and to possible differences in ligand coverage between these samples. The local vacuum energy is determined by the low kinetic energy edge in the UPS spectra, as discussed above. The low kinetic energy edge contains scattered electrons and any surface electrons with a binding energy equal to the energy of either a He(I) (20.1 eV) or He(II) (40.8 eV) photon. When a dipole layer is adsorbed to a surface, the kinetic energy of photoejected electrons can be increased or decreased as the electrons pass through the dipole layer. The magnitude of the shift in the kinetic energy of an ejected photon is dependent on two factors: (1) the ligand surface packing density and (2) the magnitude of the dipole moment of each ligand perpendicular to the surface. All of our UPS experiments were performed with the detector normal to

Table 1. Dipole Moment of Each Ligand Calculated by Spartan, Surface Work Function of Gold after Ligand Binding, Surface Work Function of Samples with Tethered CdSe NCs with Diameters 6.0 and 3.6 nm after Ligand Binding

name	calculated dipole moment of unbound ligand (D)	Work function of Au with SAM (eV)	work function on samples with 6.0 nm diameter NCs with ligand (eV)	work function on samples with 3.6 nm diameter NCs with ligand (eV)
1-hexanethiol	2.0	4.1 ± 0.1	4.1 ± 0.1	4.1 ± 0.1
1-benzenethiol	1.2	4.3 ± 0.1	4.0 ± 0.1	4.1 ± 0.1
4-fluorothiophenol	−0.6	4.9 ± 0.1	4.5 ± 0.1	4.3 ± 0.1

the surface, so only the component of the dipole moment of each ligand that is normal to the surface contributes to the measured shift in the local vacuum energy.

Samples with alkanethiol self-assembled monolayer on smooth gold have been reported to have a 30° tilt angle and only the component of the dipole moment normal to the surface affects the local vacuum energy (39, 48). For the samples with spherical NCs, it is likely that the ligands are aligned in a variety of angles as depicted in Figure 1. The smaller NCs are more curved than the larger NCs so even if both the 3.6 and 6.0 nm diameter NCs have the same ligand coverage, there would likely be a smaller fraction of ligands with their dipole moment orientated normal to the surface on the smaller NCs. Thus the difference in magnitude of changes in the work function of each surface as a function of ligand adsorption would primarily be due to increased "texturing" of the surface. We note that the shift in the local vacuum energy after adsorption of ligands is dependent on the packing density of ligands on the surface. It may be that the packing density of each ligand is lower on the more textured NC surfaces compared to smooth gold.

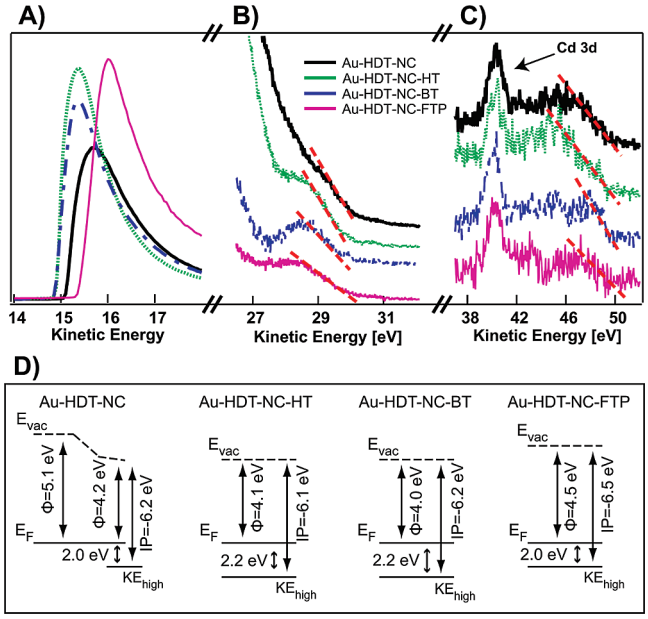

FIGURE 4. (A−C) He(I) and He(II) UPS spectra of 6.0 nm CdSe NCs tethered to template-stripped gold with 1,6-hexanedithiol. CdSe samples with no capping ligand (thick black), samples with a 1-hexanethiol (dotted green), samples with a 1-benzenethiol (dashed blue), and samples with 4-fluorothiophenol (thin purple). (A) Low kinetic energy edge, (B) background subtracted He(I) high kinetic energy edge, and (C) background subtracted He(II) high kinetic energy edge of the UPS spectra. (D) Band diagrams for each surface shown in A−C. The band diagram for bare NCs shows the shift in vacuum energy as each material is adsorbed. The other band diagrams show the NC IP, surface work function, and the offset between the NC high kinetic energy edge and the Fermi energy after each ligand is used to cap the NCs.

As mentioned earlier, shifts in the high kinetic energy of UPS spectra of CdSe NC films have been reported by Wu et al. to be influenced by final-state effects due to the NC capping ligands. Final-state effects have been proposed to explain shifts in photoemission spectra of metallic (50, 51) and semiconductor nanoparticles (30, 31) separated from metallic substrates by a insulating spacer (e.g., an organic alkanethiol self-assembled monolayer). This insulating layer can act as a barrier to charge transfer between the nanoparticles and a conductive substrate. For the tethered NC films in our study, we observed no shifts that would indicate final-state effects, but as we used the same length tether for all samples, any final-state effects, if present, would be the same for all of the samples.

Both Carlson et al. (37) and Markus et al. (52) hypothesized that the IP of CdSe NCs can be "pinned" when the NCs are tethered to a ZnO or gold electrode, due to the lack of an observed shift in the energy level offset between the high kinetic energy edge of the electrode and the high kinetic energy edge of the CdSe NCs, as a function of NC diameter. It should be noted that these studies did not reflect changes in the local vacuum energy. The interpretation of whether NC Fermi level pinning has been observed in these systems depends on how much one expects the IP of the NC to change with diameter. In our experiment, we did not expect appreciable shifts in the UPS-determined IP with NC diameter because the energy resolution of the UPS is approximately ±0.1 eV and the NCs we used have diameters of 3.6 and 6.0 nm and optical band-gaps of 2.16 and 1.97 eV, respectively. Using the effective mass approximation, we expect that the change in EA or E_{CB} is 3.5 times larger than the change in IP, so shifts in the IP for the NCs we used might be difficult to quantify if they occur (53, 54).

In our analysis, we have defined the surface work function and the NC IP relative the local vacuum energy. This is an important distinction. Other groups have referenced the high kinetic energy edge of NC spectra to bulk semiconductor samples or to the work function or IP of the surface to which the NCs are attached (29−32, 37, 52). This can lead to incorrect calculations of the NC IP. For example, for the NCs in our sample, the energy offset between the high kinetic energy edge of the NCs relative to the Fermi energy of the gold substrate is 2.0−2.2 eV. The work function of gold is 5.1 eV; thus if we calculated the NC IP relative to the Fermi energy of gold (without accounting for shifts in the

Table 2. Dipole Moment of Each Ligand Calculated by Spartan, Surface Work Function of Gold, IP of 6.0 nm NCs, and IP of 3.6 nm NCs after Ligand Binding

name	calculated dipole moment of unbound ligand (D)	work function of Au with SAM (eV)	6.0 nm NC IP with ligand (eV)	3.6 nm IP NCs with ligand (eV)
1-hexanethiol	2.0	4.1 ± 0.1	6.1 ± 0.1	6.2 ± 0.1
1-benzenethiol	1.2	4.3 ± 0.1	6.2 ± 0.1	6.3 ± 0.1
4-fluorothiophenol	−0.6	4.9 ± 0.1	6.5 ± 0.1	6.3 ± 0.1

local vacuum energy), we could calculate NC IPs of 7.1−7.3 eV. In UPS experiments, it is important to recognize that the Fermi energy throughout a sample is constant (i.e., electronic equilibrium is maintained between the sample and the spectrometer), but that the local vacuum energy shifts (46, 47).

We have shown that the ligand effects on NC IP and the local surface work function can be discussed by separating the shifts in the local vacuum energy of the surface and the high kinetic energy edge of the NCs. We find that for the ligands examined here, the largest effects are changes in the local vacuum energy, suggesting that we can tune the energy level offsets between colloidal NCs and other materials for use in electronic devices. This would be comparable to tuning the work function of macroscopic surfaces like ITO or gold by the addition of a dipole layer (38, 39, 41). If capping ligands with properly tuned substituents can be used to control effective local work function or the frontier orbital energy levels, it may be possible to control rates of electron transfer in both OLED and OPV applications of functional NC materials. Large IPs have been assumed for CdSe NCs in polymer hosts or small molecule matrices (e.g., 6.4 eV is commonly used as the IP of CdSe NCs) (1, 9). Such large IPs would appear to make their use as emissive dopants in OLEDs problematic for hole-injection, because the host material rarely has an IP that large (1, 4, 9, 55, 56). In addition, NC-doped OPVs are currently less efficient than all-organic PVs, which may be due to the HOMO−HOMO and LUMO−LUMO offsets between commonly used p-type organic polymers and II−VI NCs (57, 58). The work reported here provides a way to characterize the IP of NC films at the microscopic level by UPS of tethered monolayers, accounting for changes in both the high kinetic energy edge and the local vacuum energy. Future studies are focusing on how the surface work function and IP of tethered CdSe NCs, core−shell NCs, and related II−VI and III−V NCs shift due to capping ligands with different binding groups, and how the charge transfer between NCs and polymers can be affected by these surface ligands in an environment comparable to a solid-state device (9, 36, 55, 56).

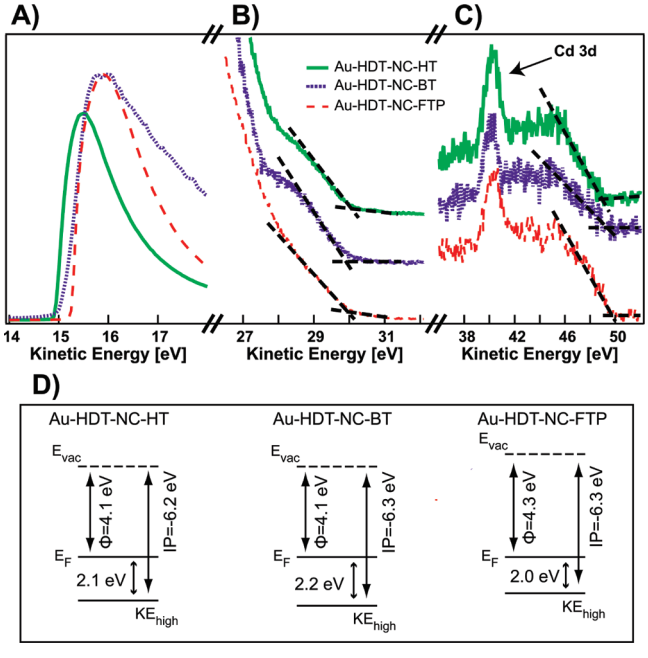

FIGURE 5. (A−C) He(I) and He(II) UPS spectra of 3.6 nm CdSe NCs tethered to template-stripped gold with 1,6-hexanedithiol. CdSe samples with 1-hexanethiol (thick green), samples with a 1-benzenethiol (dotted purple), and samples with 4-fluorothiophenol (dashed red). (A) Low kinetic energy edge, (B) background subtracted He(I) high kinetic energy edge, and (C) background subtracted He(II) high kinetic energy edge of the UPS spectra. (D) Band diagrams for each surface shown in A−C. The band diagrams show the NC IP, surface work function, and the offset between the NC high kinetic energy edge and the Fermi energy after each ligand is used to cap the NCs.

Acknowledgment. This work was supported in part by the Division of Chemical Science, Geosciences, and Bioscience, Office of Basic Energy Sciences of the U.S. Department of Energy, through Grant DE-FG03-92ER15753, the Office of Naval Research and by the National Science Foundation CHE-0517963, and the NSF Science and Technology Center Materials and Devices for Information Technology DMR-012097. A.M.M. gratefully acknowledges the National Science Foundation for funding of an NSF-ACC postdoctoral fellowship under CHE-0836096.

Supporting Information Available: X-ray photoelectron spectra, AFM micrographs of samples, details of dipole moment calculations, and further details about IP calculations (PDF). This material is available free of charge via the Internet at http://pubs.acs.org.

REFERENCES AND NOTES

(1) Coe, S.; Woo, W. K.; Bawendi, M.; Bulovic, V. *Nature* **2002**, *420*, 800–803.
(2) Colvin, V. L.; Schlamp, M. C.; Alivisatos, A. P. *Nature* **1994**, *370*, 354–357.
(3) Dabbousi, B. O.; Bawendi, M. G.; Onitsuka, O.; Rubner, M. F. *Appl. Phys. Lett.* **1995**, *66*, 1316–1318.
(4) Zhao, J. L.; Bardecker, J. A.; Munro, A. M.; Liu, M. S.; Niu, Y. H.; Ding, I. K.; Luo, J. D.; Chen, B. Q.; Jen, A. K. Y.; Ginger, D. S. *Nano Lett.* **2006**, *6*, 463–467.
(5) Greenham, N. C.; Peng, X. G.; Alivisatos, A. P. *Phys. Rev. B* **1996**, *54*, 17628–17637.
(6) Huynh, W. U.; Dittmer, J. J.; Alivisatos, A. P. *Science* **2002**, *295*, 2425–2427.
(7) Anderson, I. E.; Breeze, A. J.; Olson, J. D.; Yang, L.; Sahoo, Y.; Carter, S. A. *Appl. Phys. Lett.* **2009**, *94*, 063101.
(8) Gur, I.; Fromer, N. A.; Geier, M. L.; Alivisatos, A. P. *Science* **2005**, *310*, 462–465.

(9) Anikeeva, P. O.; Halpert, J. E.; Bawendi, M. G.; Bulovic, V. *Nano Lett.* **2009**, *9*, 2532–2536.
(10) Saunders, B. R.; Turner, M. L. *Adv. Colloid Interface Sci.* **2008**, *138*, 1–23.
(11) Shalom, M.; Ruhle, S.; Hod, I.; Yahav, S.; Zaban, A. *J. Am. Chem. Soc.* **2009**, *131*, 9876–9877.
(12) Soreni-Harari, M.; Yaacobi-Gross, N.; Steiner, D.; Aharoni, A.; Banin, U.; Millo, O.; Tessler, N. *Nano Lett.* **2008**, *8*, 678–684.
(13) Steiner, D.; Dorfs, D.; Banin, U.; Della Sala, F.; Manna, L.; Millo, O. *Nano Lett.* **2008**, *8*, 2954–2958.
(14) Brus, L. E. *J. Chem. Phys.* **1983**, *79*, 5566–5571.
(15) Chen, Y.; Vela, J.; Htoon, J.; Casson, J. L.; Werder, D. J.; Bussian, D. A.; Klimov, V. I.; Hollingsworth, J. A. *J. Am. Chem. Soc.* **2008**, *130*, 5026.
(16) Gao, X. H.; Cui, Y. Y.; Levenson, R. M.; Chung, L. W. K.; Nie, S. M. *Nat. Biotechnol.* **2004**, *22*, 969–976.
(17) Guyot-Sionnest, P.; Wehrenberg, B.; Yu, D. *J. Chem. Phys.* **2005**, *123*, 074709.
(18) Pandey, A.; Guyot-Sionnest, P. *Science* **2008**, *322*, 929–932.
(19) Rabani, E.; Hetenyi, B.; Berne, B. J.; Brus, L. E. *J. Chem. Phys.* **1999**, *110*, 5355–5369.
(20) Smith, A. M.; Nie, S. *Acc. Chem. Res.* **2010**, *43*, 190–200.
(21) Bruchez, M.; Moronne, M.; Gin, P.; Weiss, S.; Alivisatos, A. P. *Science* **1998**, *281*, 2013–2016.
(22) Chan, W. C. W.; Nie, S. M. *Science* **1998**, *281*, 2016–2018.
(23) Kalyuzhny, G.; Murray, R. W. *J. Phys. Chem. B* **2005**, *109*, 7012–7021.
(24) Munro, A. M.; Plante, I. J. L.; Ng, M. S.; Ginger, D. S. *J. Phys. Chem. C* **2007**, *111*, 6220–6227.
(25) Talapin, D. V.; Rogach, A. L.; Kornowski, A.; Haase, M.; Weller, H. *Nano Lett.* **2001**, *1*, 207–211.
(26) Ginger, D. S.; Greenham, N. C. *J. Appl. Phys.* **2000**, *87*, 1361–1368.
(27) Jarosz, M. V.; Porter, V. J.; Fisher, B. R.; Kastner, M. A.; Bawendi, M. G. *Phys. Rev. B* **2004**, *70*, 195327.
(28) Talapin, D. V.; Murray, C. B. *Science* **2005**, *310*, 86–89.
(29) Colvin, V. L.; Alivisatos, A. P.; Tobin, J. G. *Phys. Rev. Lett.* **1991**, *66*, 2786–2789.
(30) Wu, P. J.; Tsuei, K. D.; Wei, K. H.; Liang, K. S. *Solid State Commun.* **2007**, *141*, 6–11.
(31) Wu, P. J.; Tsuei, K. D.; Hsieh, M. T.; Wei, K. H.; Liang, K. S. *Phys. Rev. B* **2007**, *75*, 115402.
(32) Meulenberg, R. W.; Lee, J. R. I.; Wolcott, A.; Zhang, J. Z.; Terminello, L. J.; van Buuren, T. *ACS Nano* **2009**, *3*, 325–330.
(33) Guyot-Sionnest, P. *Microchimica Acta* **2008**, *160*, 309–314.
(34) Wang, C. J.; Shim, M.; Guyot-Sionnest, P. *Science* **2001**, *291*, 2390–2392.
(35) Bard, A. J.; Faulkner, L. R. *Electrochemical Methods Fundamentals and Applications*, 2nd ed.; John Wiley & Sons: New York, 2001.
(36) Campbell, I. H.; Crone, B. K. *Appl. Phys. Lett.* **2008**, *92*, 043303.
(37) Carlson, B.; Leschkies, K.; Aydil, E. S.; Zhu, X.-Y. *J. Phys. Chem. C* **2008**, *112*, 8419–8423.
(38) Alloway, D. M.; Graham, A. L.; Yang, X.; Mudalige, A.; Colorado, J. R.; Wysocki, V. H.; Pemberton, J. E.; Lee, T. R.; Wysocki, R. J.; Armstrong, N. R. *J. Phys. Chem. C* **2009**, *113*, 20328–20334.
(39) Alloway, D. M.; Hofmann, M.; Smith, D. L.; Gruhn, N. E.; Graham, A. L.; Colorado, J. R.; Wysocki, V. H.; Lee, T. R.; Lee, P. A.; Armstrong, N. R. *J. Phys. Chem. B* **2003**, *107*, 11690–11699.
(40) Hotchkiss, P. J.; Hong, L.; Pavel, B. P.; Sergio, A. P.; Simon, C. J.; Neal, R. A.; Jean-Luc, B.; Seth, R. M. *Adv. Mater.* **2009**, *21*, 1–6.
(41) Paniagua, S. A.; Hotchkiss, P. J.; Jones, S. C.; Marder, S. R.; Mudalige, A.; Marrikar, F. S.; Pemberton, J. E.; Armstrong, N. R. *J. Phys. Chem. C* **2008**, *112*, 7809–7817.
(42) Paramonov, P. B.; Paniagua, S. A.; Hotchkiss, P. J.; Jones, S. C.; Armstrong, N. R.; Marder, S. R.; Bredas, J. L. *Chem. Mater.* **2008**, *20*, 5131–5133.
(43) Yu, W. W.; Qu, L. H.; Guo, W. Z.; Peng, X. G. *Chem. Mater.* **2003**, *15*, 2854–2860.
(44) Shallcross, R. C.; D'Ambruoso, G. D.; Korth, B. D.; Hall, H. K.; Zheng, Z. P.; Pyun, J.; Armstrong, N. R. *J. Am. Chem. Soc.* **2007**, *129*, 11310–11311.
(45) Naumann, R.; Schiller, S. M.; Giess, F.; Grohe, B.; Hartman, K. B.; Karcher, I.; Koper, I.; Lubben, J.; Vasilev, K.; Knoll, W. *Langmuir* **2003**, *19*, 5435–5443.
(46) Cahen, D.; Kahn, A. *Adv. Mater.* **2003**, *15*, 271–277.
(47) Ishii, H.; Sugiyama, K.; Ito, E.; Seki, K. *Adv. Mater.* **1999**, *11*, 972–972.
(48) Heimel, G.; Romaner, L.; Zojer, E.; Bredas, J.-L. *Acc. Chem. Res.* **2008**, *41*, 721–729.
(49) Katari, J. E. B.; Colvin, V. L.; Alivisatos, A. P. *J. Phys. Chem.* **1994**, *98*, 4109–4117.
(50) Boyen, H.-G.; Ethirajan, A.; Kastle, G.; Weigl, F.; Ziemann, P.; Schmid, G.; Garnier, M. G.; Buttner, M.; Oelhafen, P. *Phys. Rev. Lett.* **2005**, *94*, 016804.
(51) Wertheim, G. K.; Dicenzo, S. B.; Youngquist, S. E. *Phys. Rev. Lett.* **1983**, *51*, 2310–2313.
(52) Markus, T. Z.; Wu, M.; Wang, L.; Waldeck, D. H.; Oron, D.; Naaman, R. *J. Phys. Chem. C* **2009**, *113*, 14200–14206.
(53) Brus, L. *J. Phys. Chem.* **1986**, *90*, 2555–2560.
(54) Efros, A. L.; Rosen, M. *Annu. Rev. Mater. Sci.* **2000**, *30*, 475–521.
(55) Chin, P. T. K.; Hikmet, R. A. M.; Janssen, R. A. J. *J. Appl. Phys.* **2008**, *104*, 013108.
(56) Munro, A. M.; Bardecker, J. A.; Liu, M. S.; Cheng, Y. J.; Niu, Y. H.; Plante, I. J. L.; Jen, A. K. Y.; Ginger, D. S. *Microchimica Acta* **2008**, *160*, 345–350.
(57) Milliron, D. J.; Alivisatos, A. P.; Pitois, C.; Edder, C.; Frechet, J. M. J. *Adv. Mater.* **2003**, *15*, 58–61.
(58) Noone, K. M.; Anderson, N. C.; Horwitz, N. E.; Munro, A. M.; Kulkarni, A. P.; Ginger, D. S. *ACS Nano* **2009**, *3*, 1345–1352.

AM900834Y